Formation Flying Orbit and Control Concept for Virtual Super Optics Reconfigurable Swarm Mission

Adam W. Koenig* and Simone D'Amico†
Stanford University, Stanford, California 94305
and
E. Glenn Lightsey‡
Georgia Institute of Technology, Atlanta, Georgia 30332

https://doi.org/10.2514/1.G007334

The Virtual Super Optics Reconfigurable Swarm (VISORS) mission is a distributed telescope consisting of two 6U CubeSats separated by 40 m that will obtain high-resolution images of active solar regions in the extreme ultraviolet spectrum. This mission is challenging because the CubeSats must autonomously control their relative motion with unprecedented accuracy while operating in close proximity. This paper presents three contributions that enable the VISORS mission to meet its challenging requirements. First, passively safe absolute and relative orbit designs for distributed telescopes that provide regular periods of alignment with inertial targets are developed using relative eccentricity/inclination vector separation. Second, a guidance, navigation, and control system design is proposed to meet the demanding relative motion control requirements. Third, a concept of operations is proposed that minimizes mission operations load when the formation is not actively performing observations. This concept of operations includes a safety plan to address on-orbit anomalies. The performance of the guidance, navigation, and control system is validated through Monte Carlo simulations including all significant error sources and operational constraints. These simulations show that the mission requirements are met with margin, providing a preliminary demonstration of the feasibility of accurate autonomous formation control with CubeSats.

I. Introduction

DISTRIBUTED space systems are an active research area in recent years due to their ability to achieve objectives that are difficult or impossible to achieve with a monolithic spacecraft. Indeed, the capabilities of distributed space systems are evident from the successes of missions such as Gravity Recovery and Climate Experiment (GRACE) [1], TerraSAR-X add-on for Digital Elevation Measurement (TanDEM-X) [2], and Magnetospheric MultiScale mission (MMS) [3]. However, these missions required large spacecraft and budgets of hundreds of millions of dollars. In an effort to reduce costs, researchers have recently focused on development of subsystems such as star tracker sensors [4], navigation systems [5], and propulsion systems [6] for CubeSats that narrow the performance gap between nanosatellites and flagship-class spacecraft.

Leveraging these developments, the Virtual Super Optics Reconfigurable Swarm (VISORS) mission was proposed in the NSF IdeasLab [7] to gather high-resolution images of the sun in the extreme ultraviolet spectrum. The collected data will be used to improve thermodynamic models of the solar corona. The space segment of the VISORS mission is a distributed telescope consisting of two 6U CubeSats: an optics spacecraft (OSC) and a detector spacecraft (DSC). The optics spacecraft hosts a photon sieve payload that acts as a high-resolution lens in the extreme ultraviolet spectrum. The deployable solar panels double as a sunshade, blocking most of the light from regions outside the area of interest from reaching the DSC. The DSC hosts a detector payload that collects focused images produced by the photon sieve. A conceptual illustration of the distributed telescope performing an observation is shown in Fig. 1.

The VISORS mission is challenging because the relative motion of the spacecraft must be autonomously controlled with higher accuracy than other distributed telescopes such as Proba-3 [8] or the miniaturized distributed occulter/telescope [9] using smaller and less expensive spacecraft. The three requirements that the relative motion must satisfy throughout each successful science observation (of 10 s duration) are as follows:

1) *Alignment with active region:* The relative position of the center of the photon sieve pattern must not deviate from the line from the center of the detector aperture to the center of the target active region by more than 18 mm.

2) *Line of sight stability:* The inertial relative velocity of the spacecraft in the plane perpendicular to the line of sight must not exceed 0.2 mm/s to ensure that common features can be tracked across exposures.

3) *Focus:* The separation between the center of the detector aperture and the center of the photon sieve pattern must remain within 15 mm of the target separation (nominally 40 m) to ensure that collected images are in focus.

The constraints on the relative motion imposed by these requirements are illustrated in Fig. 2. In this figure, the red cylinder shows an example envelope that the relative position vector must remain inside for a single observation. Instead, the black cylinder shows the boundary of the admissible region for the relative position vector in all observations of a specified active region of the sun.

It is obvious that these requirements can only be met using autonomous navigation and control. However, current navigation systems with sufficient accuracy to ensure that every observation attempt is successful (e.g., LIDAR or laser metrology) are not compatible with the mass, power, and volume constraints of a CubeSat platform. Because only one successful observation is needed for VISORS mission success, the project team has posed a requirement that the Guidance, Navigation, and Control (GNC) system provides sufficient navigation and control accuracy to ensure that 20% of all science observation attempts are successful. This value was selected to provide a 99% likelihood of achieving mission success with only 20 observation attempts. Similarly, it is 90% likely that a set of 10 observation attempts will include at least one successful observation. Additionally, it is feasible to meet this requirement using differential carrier-phase

Presented as Paper 2021-0423 at the AIAA SciTech 2021 Forum, Virtual Event, January 11–21, 2021; received 29 October 2022; revision received 30 March 2023; accepted for publication 3 April 2023; published online 9 June 2023.

*Postdoctoral Scholar, Department of Aeronautics and Astronautics, Durand Building, 496 Lomita Mall. Member AIAA.

†Assistant Professor, Department of Aeronautics and Astronautics, Durand Building, 496 Lomita Mall. Fellow AIAA.

‡Professor, Georgia Tech Center for Space Technology and Research, Montgomery Knight Building, 270 Ferst Drive, 620 Cherry Street NW. Fellow AIAA.

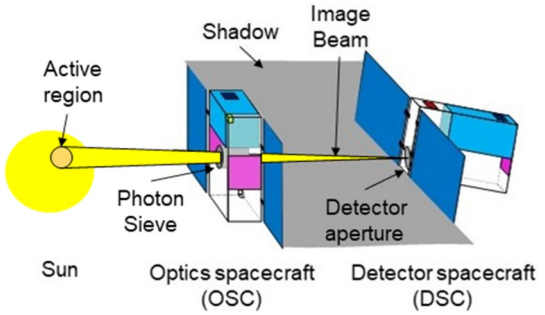

Fig. 1 Conceptual illustration of VISORS distributed telescope during observations.

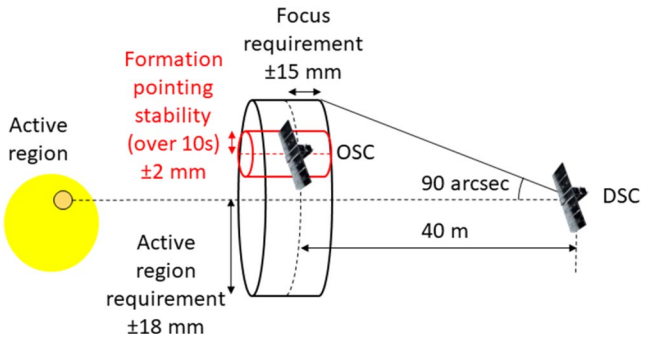

Fig. 2 Illustration of the three requirements posed on formation geometry during science observations.

Global Navigation Satellite System (GNSS) navigation techniques [5], which are suitable for deployment on CubeSats.

In addition to the observation requirements, the VISORS mission is subject to two key operational constraints. First, translational maneuvers cannot be performed during science observations because both spacecraft are subject to stringent attitude stability requirements. It follows that the absolute and relative orbits must be designed to minimize the lateral relative acceleration (i.e., relative acceleration in the plane perpendicular to the telescope boresight) during observations. Second, it is necessary to ensure that the relative orbits are passively safe for as long as possible (≥2 orbits) to allow time for an active collision avoidance maneuver in the case of anomalies. Since the evolution of the along-track separation is subject to high uncertainty under the effects of differential drag, this is best accomplished using relative eccentricity/inclination vector separation [10]. This approach provides a minimum separation in the plane perpendicular to the flight direction that varies slowly under the effects of perturbations.

This paper makes three contributions to the state-of-the-art to address challenges associated with the VISORS mission, distributed telescopes in Earth orbit, and other CubeSat missions that require accurate autonomous formation control. First, it is demonstrated that a family of relative orbits developed using relative eccentricity/inclination vector separation are optimal for distributed telescope applications. These orbit designs simultaneously provide periods of passive alignment with inertial targets and at least several orbits of passive safety with separations as small as tens of meters. Second, a preliminary design of a GNC system capable of meeting the challenging VISORS mission requirements is proposed. Third, a concept of operations for the VISORS mission is presented that minimizes mission operations load when the formation is not actively attempting science observations. The VISORS mission design leverages algorithms and approaches with flight heritage on PRISMA [11], TanDEM-X [12], and other missions whenever possible. The performance of the GNC system is assessed through high-fidelity Monte Carlo simulations, including all major error sources and operational constraints affecting the mission. The simulation results demonstrate the feasibility of meeting the challenging requirements of the VISORS mission and achieving accurate autonomous formation control using CubeSats.

After this introduction, Sec. II describes mathematical preliminaries that are used throughout the paper. Next, Sec. III describes the orbit design and passive safety error budget. Section IV describes the hardware and software used in the GNC system, and Sec. V describes the GNC behaviors in each operations mode. Finally, the Monte Carlo simulations used to assess performance are described in Sec. VI, and conclusions are summarized in Sec. VII.

II. Mathematical Preliminaries

The relative orbit of the VISORS formation is described in terms of relative orbital elements (ROEs). Specifically, the chosen state definition is the quasi-nonsingular ROE adopted in [11], which are defined as functions of the Keplerian orbit elements of the OSC (denoted by subscript o) and DSC (denoted by subscript d) as

$$\begin{pmatrix} \delta a \\ \delta\lambda \\ \delta e_x \\ \delta e_y \\ \delta i_x \\ \delta i_y \end{pmatrix} = \begin{pmatrix} \delta a \\ \delta\lambda \\ \delta e\cos(\phi) \\ \delta e\sin(\phi) \\ \delta i\cos(\psi) \\ \delta i\sin(\psi) \end{pmatrix} = \begin{pmatrix} \dfrac{a_o - a_d}{a_d} \\ (M_o - M_d) + (\omega_o - \omega_d) + \cos(i_d)(\Omega_o - \Omega_d) \\ e_o\cos(\omega_o) - e_d\cos(\omega_d) \\ e_o\sin(\omega_o) - e_d\sin(\omega_d) \\ i_o - i_d \\ \sin(i_d)(\Omega_o - \Omega_d) \end{pmatrix} \tag{1}$$

where a denotes the semimajor axis, e denotes the eccentricity, i denotes the inclination, Ω denotes the right ascension of the ascending node (RAAN), ω denotes the argument of perigee, and M denotes the mean anomaly. This state definition is adopted for two reasons. First, it has a simple geometric relationship with the relative motion in the local radial/tangential/normal (RTN) frame as shown in Fig. 3. The radial direction is parallel to the OSC's position vector, the normal direction is aligned with the OSC's angular momentum vector, and the tangential direction completes the right-handed triad. Second, accurate closed-form linear dynamics models such as those in [13] have been derived for this state definition, which in turn allow use of globally optimal maneuver planning algorithms for linear systems [14].

III. Optimal and Safe Orbit Design

The orbit design for the VISORS mission is driven by the need to simultaneously 1) satisfy the relative motion control requirements during observations and 2) ensure passively safe relative motion to provide time for collision avoidance maneuvers in contingency scenarios. It is additionally desirable to ensure that the relative motion during observations is periodic to minimize station-keeping Δv costs.

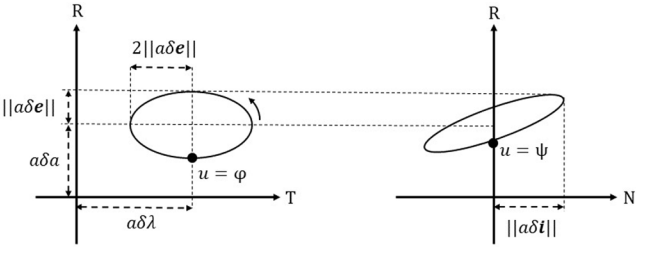

Fig. 3 Illustration of relationship between relative orbital elements (ROEs) and relative motion in the RTN frame in near-circular orbits.

The formation pointing stability requirement is nearly 10 times stricter than the other two requirements during observations and drives the orbit design. To satisfy this requirement over a 10 s observation, it is imperative to minimize the lateral relative acceleration between the spacecraft during observations. Neglecting the effects of perturbations, the lateral relative acceleration is minimized if the positions of the OSC and DSC (denoted $\boldsymbol{r}_o$ and $\boldsymbol{r}_d$, respectively) are selected to satisfy

$$\left(\frac{\mu}{\|\boldsymbol{r}_o\|^2}-\frac{\mu}{\|\boldsymbol{r}_d\|^2}\right)\cdot\left(\frac{\boldsymbol{r}_o-\boldsymbol{r}_d}{\|\boldsymbol{r}_o-\boldsymbol{r}_d\|}\right)=0 \tag{2}$$

where μ is the gravitational parameter of the central body. As shown in [9], this equation has two classes of solutions given by

$$\boldsymbol{r}_o=\alpha\boldsymbol{r}_d \quad \text{or} \quad \|\boldsymbol{r}_o\|=\|\boldsymbol{r}_d\| \tag{3}$$

The first class of solutions consists of formations aligned in the radial direction. However, since the inertial relative velocity of the spacecraft must be zero, this results in a formation with a nonzero relative semimajor axis. Accordingly the natural relative motion is not periodic and requires substantial station-keeping Δv costs. It is evident from these properties that radial alignment is an impractical choice for distributed telescopes.

The second class of solutions includes all configuration where the OSC and DSC have the same orbit radius. It follows that the formation is aligned in the tangential/normal plane of the RTN frame. However, for an observation it is necessary to ensure that the lateral relative acceleration remains small throughout on observation of at least 10 seconds. To ensure that the passive relative motion accounts for no more than 25% of the relative velocity control error budget, it is considered acceptable to perform observations in windows where the lateral relative acceleration is no larger than 5 $\mu\text{m/s}^2$. Using the expression on the left side of Eq. (3), this condition is satisfied at the nominal separation of 40 m as long as the relative position vector is within two degrees of the tangential/normal (TN) plane. The drift caused by the longitudinal (i.e., along the telescope boresight) relative acceleration over a 10 s observation will not exceed 3 mm (assuming a separation of 40 m), which is small relative to the focus requirement.

With these considerations in mind, it is useful to consider the behavior of the pointing vector to a target active region of the sun in the RTN frame. Figure 4 shows the evolution of the pointing vector to a target region for various β angles (β is the angle between the pointing vector to the target region and its projection onto the orbit plane). It is clear from this plot that there are at least two locations on any orbit at which the pointing vector to a target region of the sun must lie in the TN plane (see gray plane in Fig. 4). No assumptions on the absolute orbit are made in this plot, though it should be noted that β can slowly vary over the orbit due to the effects of perturbations.

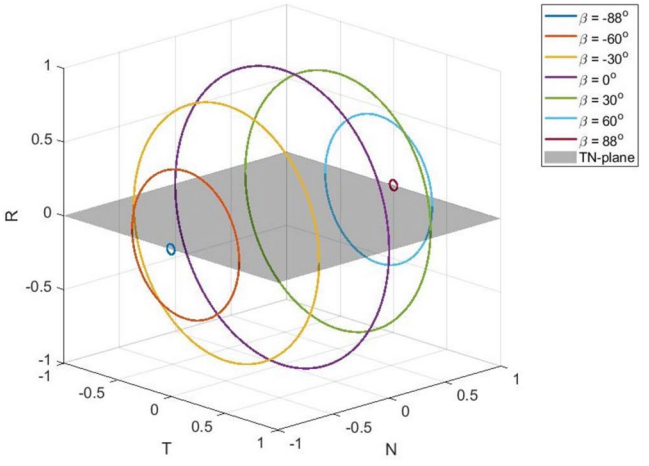

Fig. 4 Evolution of the pointing vector to an inertial target in the RTN frame over one orbit for selected beta angles with TN plane shown in gray.

The rate of change of the pointing vector to any inertial target in the RTN frame is bounded by the angular velocity of the orbit, which is 0.0011 rad/s (0.063 deg/s) in low Earth orbit and decreases with increasing orbit radius. Accordingly, the windows in which the pointing vector lies within two degrees of the TN plane must be at least 1 minute in duration in low Earth orbit. The duration of these windows increases with both β and the orbit radius, but the duration of an observation remains limited by the longitudinal relative acceleration. Overall, this analysis shows that there exist at least windows in any Earth orbit where the natural relative motion can satisfy the VISORS observation requirements for at least 10 s.

Next, it is necessary to derive constraints that ensure that the relative motion is passively safe. To accomplish this, it is helpful to first compute the families of relative orbits that provide alignment with an inertial target with zero lateral relative acceleration. The possible values of the relative position $\delta\boldsymbol{r}$ and relative velocity $\delta\boldsymbol{v}$ in the RTN frame that simultaneously provide 1) alignment with a target in the TN plane and 2) zero relative velocity in the inertial frame are given by

$$\begin{pmatrix}\delta r_R\\ \delta r_T\\ \delta r_N\\ \delta v_R\\ \delta v_T\\ \delta v_N\end{pmatrix}=\begin{pmatrix}0\\ s\cos(\beta)\\ \pm\, s\sin(\beta)\\ \dot{\nu}s\cos(\beta)\\ 0\\ 0\end{pmatrix} \quad \text{or} \quad \begin{pmatrix}0\\ -s\cos(\beta)\\ \pm\, s\sin(\beta)\\ -\dot{\nu}s\cos(\beta)\\ 0\\ 0\end{pmatrix} \tag{4}$$

where s is the separation and $\dot{\nu}$ is the rate of change of the true anomaly. In near-circular orbits, these solutions can be converted to ROE using the linear relationship given by D'Amico [11] as

$$\begin{pmatrix}\delta r_R\\ \delta r_T\\ \delta r_N\\ \delta v_R\\ \delta v_T\\ \delta v_N\end{pmatrix}=a\begin{bmatrix}1 & 0 & -\cos(u) & -\sin(u) & 0 & 0\\ 0 & 1 & 2\sin(u) & -2\cos(u) & 0 & 0\\ 0 & 0 & 0 & 0 & \sin(u) & -\cos(u)\\ 0 & 0 & n\sin(u) & -n\cos(u) & 0 & 0\\ -1.5n & 0 & 2n\cos(u) & 2n\sin(u) & 0 & 0\\ 0 & 0 & 0 & 0 & \cos(u) & \sin(u)\end{bmatrix}\times\begin{pmatrix}\delta a\\ \delta\lambda\\ \delta e_x\\ \delta e_y\\ \delta i_x\\ \delta i_y\end{pmatrix} \tag{5}$$

where n denotes the mean motion of the orbit and $u=\omega+M$ is the mean argument of latitude. Using this relationship, it is possible to convert the relative positions and velocity solutions in Eq. (4) to ROE solutions as given by

$$\begin{pmatrix}\delta a\\ \delta\lambda\\ \delta e_x\\ \delta e_y\\ \delta i_x\\ \delta i_y\end{pmatrix}=\frac{1}{a}\begin{pmatrix}0\\ -s\cos(\beta)\\ s\cos(\beta)\sin(u)\\ -s\cos(\beta)\cos(u)\\ \pm\, s\sin(\beta)\sin(u)\\ \pm\, s\sin(\beta)\cos(u)\end{pmatrix} \quad \text{or} \quad \frac{1}{a}\begin{pmatrix}0\\ s\cos(\beta)\\ -s\cos(\beta)\sin(u)\\ s\cos(\beta)\cos(u)\\ \pm\, s\sin(\beta)\sin(u)\\ \pm\, s\sin(\beta)\cos(u)\end{pmatrix} \tag{6}$$

All of these solutions provide (anti-)parallel relative eccentricity and relative inclination vectors. It follows that passive safety can be

established using the well-known relative eccentricity/inclination vector separation concept [10], which ensures a user-specified minimum separation in the plane perpendicular to the flight direction. However, it is still necessary to ensure that the individual magnitudes of the relative eccentricity and inclination vector are large enough to ensure a safe minimum separation in the presence of all error sources (navigation, control, and perturbations). The nominal magnitudes of the relative eccentricity and inclination vectors for all solutions to Eq. (6) are given by

$$\|a\delta\boldsymbol{e}\| = s\cos(\beta)\|a\delta\boldsymbol{i}\| = s\sin(\beta) \tag{7}$$

Because $\delta\boldsymbol{e}$ and $\delta\boldsymbol{i}$ are (anti-)parallel and the nominal δa is zero, it is possible to reformulate the expression for the minimum separation in the radial/normal (RN) plane (denoted $s_{\mathrm{RN,min}}$) provided in [10] as

$$s_{\mathrm{RN,min}} = \min(|s\cos(\beta)| - \delta r_{R,\mathrm{err}}, |s\sin(\beta)| - \delta r_{N,\mathrm{err}}) \tag{8}$$

where and $\delta r_{R,\mathrm{err}}$ and $\delta r_{N,\mathrm{err}}$ are the changes in the radial and normal components of the relative position vector due to all error sources. For specified error values and a minimum safe RN plane separation ϵ_{RN}, the constraints imposed on β can be posed as

$$\beta \le \cos^{-1}\left(\frac{\epsilon_{\mathrm{RN}} + \delta r_{R,\mathrm{err}}}{s}\right), \quad \beta \ge \sin^{-1}\left(\frac{\epsilon_{\mathrm{RN}} + \delta r_{N,\mathrm{min}}}{s}\right) \tag{9}$$

It is evident from this equation that the range of admissible values of β decreases as $\delta r_{R,\mathrm{err}}$ and $\delta r_{N,\mathrm{err}}$ increase. Using the geometric relationship between the ROE and the relative position/velocity [see Eq. (5)], the radial and normal position errors can be approximated as

$$\delta r_{R,\mathrm{err}} = |a\delta a_{\mathrm{err}}| + \|a\delta\boldsymbol{e}_{\mathrm{err}}\|, \quad \delta r_{N,\mathrm{err}} = \|a\delta\boldsymbol{i}_{\mathrm{err}}\| \tag{10}$$

where $a\delta a_{\mathrm{err}}$, $a\delta\boldsymbol{e}_{\mathrm{err}}$, and $\delta\boldsymbol{i}_{\mathrm{err}}$ denote errors in the relative semimajor axis, relative eccentricity vector, and relative inclination vector, respectively. The errors in each of the ROE arise from three sources: 1) navigation, 2) control, and 3) effects of perturbations (primarily atmospheric drag in LEO). The 3-σ navigation errors from the DiGiTaL [5] algorithms that will be used on VISORS and expected control errors are provided in Table 1. The translational errors are mapped to ROE errors using the largest possible scaling factor from Eq. (5). The included control errors include the combined effects of actuation errors and deviations of the ROE from the desired passive trajectory over the complete science orbit (see Sec. VI for more details of control performance). These errors are constant for all low Earth orbits.

Atmospheric drag also contributes to $a\delta a_{\mathrm{err}}$ and $a\delta\boldsymbol{e}_{\mathrm{err}}$ and the magnitude of these contributions depends on the attitudes of the spacecraft (which affect the differential ballistic coefficient) as well as the orbit and current solar activity level (which affect the local atmospheric density). To simplify the following analysis, it is hereafter assumed that the instantaneous relative acceleration due to differential atmospheric drag d_{drag} can be expressed as a function of the local atmospheric density ρ and velocity v as given by

$$d_{\mathrm{drag}} = 0.5\rho v^2 \Delta B \quad \Delta B = 0.5|B_{\mathrm{nom}} - B_{\mathrm{avg}}| = 0.0150\ \mathrm{m^2/kg} \tag{11}$$

where ΔB is the differential ballistic coefficient, which is assumed to be constant and equal to the difference between the ballistic coefficient with the nominal attitude (B_{nom}) and the average ballistic coefficient across all possible attitudes (B_{avg}). This is consistent with a scenario in which one spacecraft is tumbling (e.g., due to an anomaly) and the other retains its nominal attitude. The values of B_{nom} and B_{avg} are given by

$$B_{\mathrm{nom}} = \frac{A_{\mathrm{nom}}C_D}{m}, \quad B_{\mathrm{avg}} = \frac{A_{\mathrm{avg}}C_D}{m} \tag{12}$$

where m is the spacecraft mass (12 kg), C_D is the drag coefficient (2.3), and A_{nom} and A_{avg} are the nominal and average cross-sectional areas of the spacecraft (0.285 and $0.206m^2$, respectively).

To develop rigorous bounds of the effects of differential drag on the relative orbit, density profiles for a wide range of low Earth orbits at epochs from 2010 to 2018 were computed using the NRLMSISE-00 atmospheric density model [15]. Using these density profiles, the cumulative effects of differential drag over two orbits on the relative semimajor axis ($a\delta a_{\mathrm{drag}}$) and the relative eccentricity vector ($a\delta\boldsymbol{e}_{\mathrm{drag}}$) were computed by numerically integrating Gauss's variational equations. Finally, these quantities were summed to compute the maximum possible decrease in the radial separation due to differential drag $\delta r_{R,\mathrm{drag}}$. Table 2 provides the worst-case values of $a\delta a_{\mathrm{drag}}$, $\|a\delta\boldsymbol{e}_{\mathrm{drag}}\|$, and $\delta r_{R,\mathrm{drag}}$ for selected altitudes in the admissible range for the VISORS mission. As atmospheric density increases exponentially as altitude decreases, establishing passive safety for at least two orbits using relative eccentricity/inclination vector separation at altitudes of less than 500 km is infeasible.

The range of safe β angles for each altitude is provided in Table 3. These values are computed using Eq. (9) for an ϵ_{RN} of 5 m and error values from Tables 1 and 2.

Since the passive safety of the formation depends strongly on β and the atmospheric density, the nominal VISORS orbit is selected to be a sun-synchronous low Earth orbit (~98° inclination), which provides slow and predictable variations in β over the year. As sun-synchronous orbits are desirable for many other missions (e.g., Earth observation), it is expected that many launch opportunities will be available. However, it is necessary to determine the acceptable range of the local time of the ascending node (LTAN). The fraction of the year during which the beta angle provides a passively safe observation geometry for a minimum RN plane separation of 5 m are shown in Fig. 5 for selected altitudes in the admissible range. It is clear from this plot that the only LTAN values that do not provide year-round observation capability are in small windows surrounding 12AM/PM (when $\beta \sim 0°$) and 6AM/PM (when $\beta \sim 90°$). The nominal LTAN for VISORS is 10AM, which provides a large radial separation for improved passive safety, but any LTAN in the range of 1–4AM/PM or 8–11AM/PM is acceptable. The nominal and acceptable ranges of the orbit parameters are provided in Table 4. However, VISORS can be deployed in any low Earth orbit with an altitude of 500–600 km as long as it provides a β within the acceptable range during science observations.

In a sun-synchronous orbit, the points at which the sun lies in the TN plane will always be within 23° of the poles due to the offset

Table 1 Navigation and control errors and corresponding effects on ROE

Source	3-σ error	$\lvert a\delta a_{\mathrm{err}}\rvert$, m	$\lVert a\delta e_{\mathrm{err}}\rVert$, m	$\lVert a\delta i_{\mathrm{err}}\rVert$, m
Navigation	3 cm	0.03	0.03	0.03
(DiGiTaL) [5]	75 μm/s	0.15	0.15	0.075
Control (SMPC)	1.5 mm/s	3	3	1.5
Total		3.18	3.18	1.58

Table 2 Effects of differential drag on ROE and radial separation for selected altitudes

Altitude, km	$\lvert a\delta a_{\mathrm{drag}}\rvert$, m	$\lVert a\delta\boldsymbol{e}_{\mathrm{drag}}\rVert$, m	$\delta r_{R,\mathrm{drag}}$
500	8.0	3.1	11.1
550	3.9	1.7	5.6
600	2.0	0.9	2.9

Table 3 Minimum and maximum safe values of β vs altitude

Altitude, km	β_{min}, deg	β_{max}, deg
500	10	55
550	10	64
600	10	69

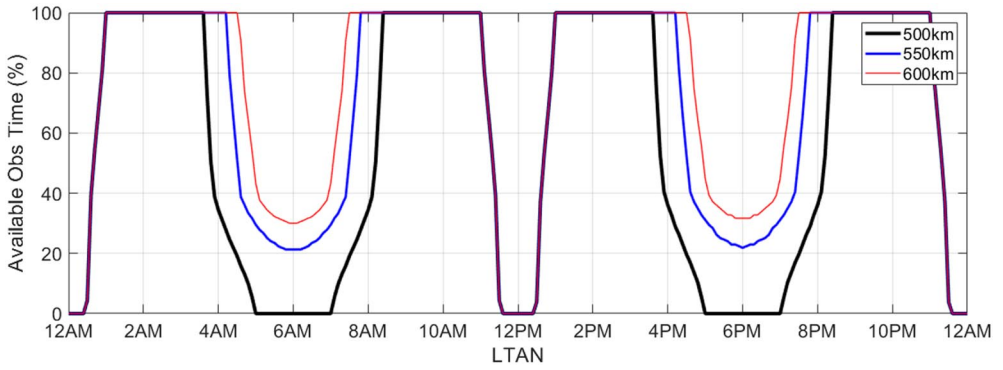

Fig. 5 Fraction of year with passively safe observations vs LTAN and altitude.

Table 4 Nominal VISORS orbit parameters and acceptable ranges

Parameter	Nominal	Acceptable range
Altitude	600 km	500–600 km
Eccentricity	0.001	< 0.01
Inclination	90°	97–99°
Argument of perigee	Any	Any
LTAN	10AM	1–4AM/PM or 8–11AM/PM
Argument of latitude for observations	90°	70–110° or 250–290°

between Earth's equatorial and ecliptic planes Accordingly, the relative eccentricity and inclination vectors will always lie within 23° of the x axis when the spacecraft are attempting observations. The exact location will depend on the time of year. Figure 6 shows the set of feasible ROE during science observations (green) accounting for this constraint and the error budgets in Tables 1 and 2. The nominal relative eccentricity and inclination vectors are indicated by black dots.

Overall, this analysis demonstrated for the first time that relative orbits designed using relative eccentricity/inclination vector separation are suitable for distributed telescopes observing inertial targets. These orbits simultaneously minimize control input required to maintain alignment and ensure a safe minimum separation in the plane perpendicular to the flight direction.

IV. Guidance, Navigation, and Control System Design

Each VISORS spacecraft consists of two parts: a spacecraft bus provided by Blue Canyon Technologies (BCT) and a payload provided by the project team. Both spacecraft have a GNC system that includes hardware and software components on the bus and payload as described in the following. An overview of the hardware layout for each spacecraft is provided in Fig. 7, and more details on the spacecraft design are provided in [16].

A. Hardware

The spacecraft bus hardware includes a star tracker, a Novatel dual frequency (L1 and L2) GNSS receiver, and a dual-frequency antenna. The GNSS antennas for both spacecraft are required to point within 30° of the zenith direction for at least one orbit before and after any observation attempt to maximize the signal-to-noise ratio of collected measurements and the number of commonly visible GNSS satellites. The payload hardware includes a near-omnidirectional intersatellite link (ISL), a 3D printed cold-gas propulsion system developed by Georgia Tech [6], and a second star tracker for the detector spacecraft (to maximize attitude stability). The ISL has a range of at least 10 km to ensure that communication is possible in a wide range of relative positions and attitudes. The propulsion module provides 8 m/s of Δv per spacecraft (16 m/s total) and has six nozzles (three opposite-facing pairs on mutually perpendicular axes), which ensure that the spacecraft can execute maneuvers in arbitrary directions without requiring attitude maneuvers. This feature enables maneuvers to be executed within 1 minute before the start of each observation, minimizing accumulated control errors. The propulsion model will have flight heritage on NASA's BioSentinel mission before the launch of VISORS.

B. Software

The GNC software will be hosted on the bus avionics board and provides two main functions: navigation and maneuver planning. The navigation software is required to provide absolute and relative orbit estimates with sufficient accuracy to enable science observations and ensure safe operations. The maneuver planning functions provide maneuver commands for station-keeping, formation reconfigurations, and collision avoidance. The navigation and maneuver

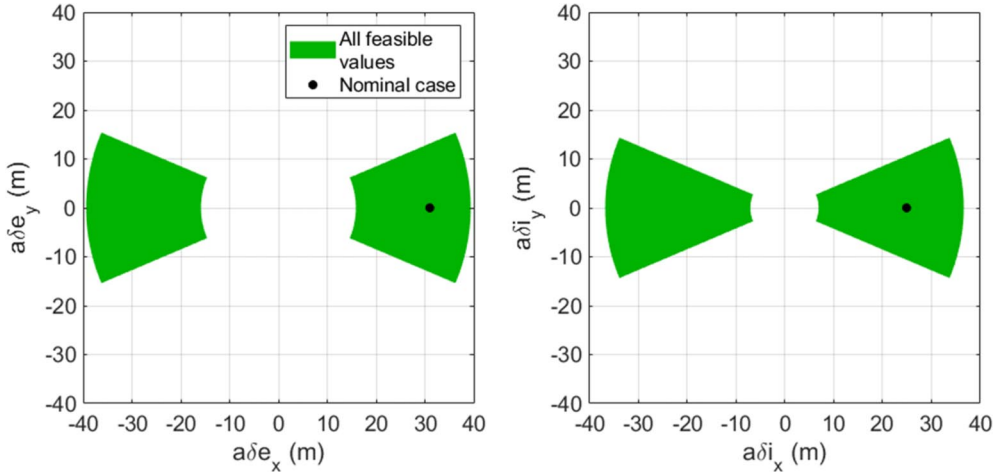

Fig. 6 Set of feasible relative eccentricity and inclination vectors (green) and nominal values (black) for science observations.

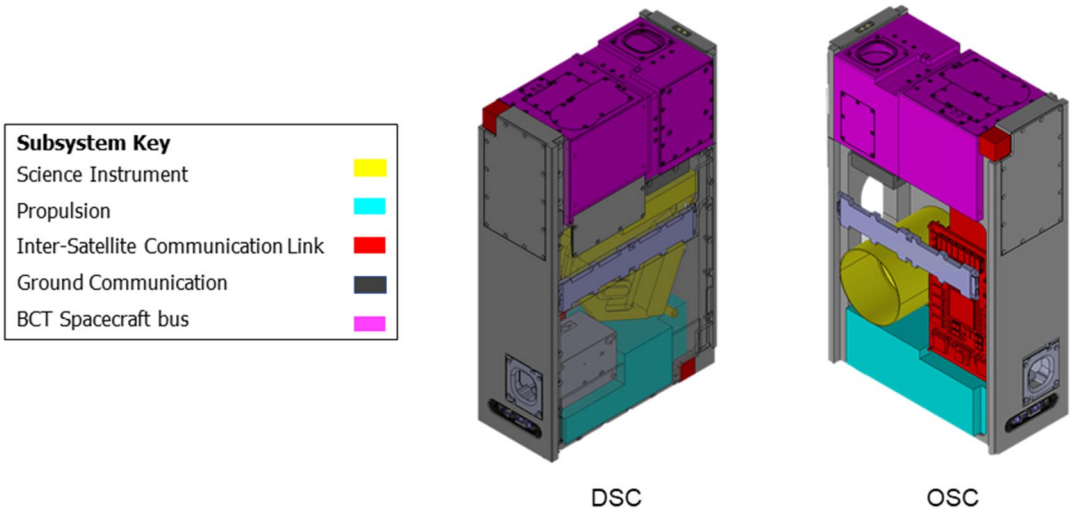

Fig. 7 Locations of key subsystems in DSC (left) and OSC (right).

planning software rely on simple algorithms with flight heritage throughout mission operations except when preparing for science observations, which require new technologies for accurate and fuel-efficient control.

A top-level view of the GNC software and its interfaces with hardware components is presented in Fig. 8. Hardware components are indicated in blue and software functions are indicated in white. During nominal operations, both spacecraft continuously exchange status data, state estimates, and raw GNSS measurements over the ISL and exchange telecommands and telemetry with the ground. The GNC software is identical on each spacecraft, but operations are distinct depending on whether the spacecraft is assigned the active "deputy" or passive "chief" role. At any time, only the deputy is allowed to autonomously plan and execute maneuvers and the chief spacecraft simply transmits measurements, state estimates, and auxiliary data while listening for anomalies. This ensures predictable behavior and safety in the event of communication outages. These roles can be autonomously exchanged if a spacecraft experiences an anomaly and are regularly exchanged by ground commands for fuel balancing.

1. *Navigation*

The navigation software provides state estimates using one of two techniques based on the separation between the spacecraft. At large separations (>100 m), the state estimates are produced using an extended Kalman filter provided with pseudorange measurements from both spacecraft, which are exchanged over the ISL. This provides relative position and velocity estimates with 1-σ (per axis) accuracy of approximately 2 m and 2 mm/s [17].

At smaller separations (<100 m and when preparing for science observations), the DiGiTaL carrier-phase differential GNSS navigation algorithms [5] are used to maximize navigation accuracy. These algorithms use raw carrier-phase and pseudorange measurements from both spacecraft to achieve relative position and velocity estimates with 1-σ accuracy (per axis) of 1 cm and 0.025 mm/s. However, these algorithms require at least one orbit of continuous measurements from commonly visible GNSS satellites to compute a solution to the integer ambiguity problem. Additionally, since the 1-σ navigation accuracy is within a factor of two of the required control accuracy during observations, it is obvious that the observation requirements can only be satisfied probabilistically. The DiGiTaL algorithms will have flight heritage on the DWARF mission before the launch of VISORS [18].

2. *Maneuver Planning*

When not actively attempting science observations, the maneuver planning algorithms use closed-form solutions with extensive flight heritage on PRISMA [11] and TanDEM-X [12]. These approaches provide highly deterministic maneuver sizes and times, ensure persistent passive safety, and have predictable Δv costs. Details on the maneuver plans used for station-keeping and formation reconfigurations are provided in Sec. V.

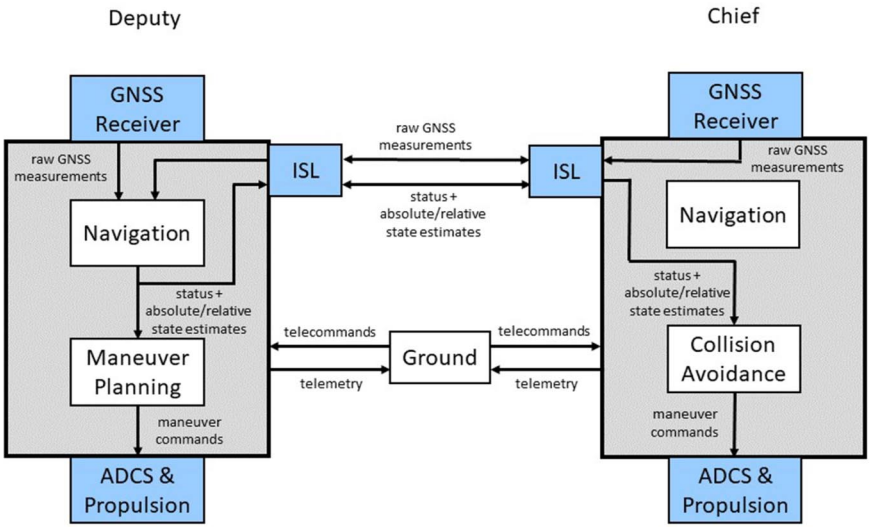

Fig. 8 Top-level view of GNC system and interfaces.

However, these closed-form solutions cannot meet the relative motion control requirements for VISORS science observations. Instead, a stochastic model predictive controller (SMPC) was developed to meet these challenging requirements subject to operational constraints and expected error sources (e.g., navigation and maneuver execution errors). At each update of the SMPC, four computations are performed:

1) The relative orbit estimate is numerically propagated to the start of next observation using the onboard dynamics model including all planned maneuvers.

2) The formal covariance of the relative state estimate is propagated to the start of the next observation using a linear dynamics model accounting for expected maneuver execution errors. Process noise of 1 m/orbit (1-σ) for each ROE is also added to produce a conservative covariance bound.

3) The desired ROEs to produce an exact alignment with the target region of the sun with zero relative velocity in the inertial frame are computed.

4) The Mahalanobis distance between the propagated and desired relative orbits is computed using the propagated covariance matrix.

5) The maneuver plan is updated if the computed Mahalanobis distance is greater than the user-specified threshold ϵ_{replan} (which is nominally set at 0.5). Otherwise the prior maneuver plan is maintained.

The threshold ϵ_{replan} ensures that computation effort is not wasted by recomputing the maneuver plan when the propagated state error is small relative to the propagated uncertainty (which decreases with the time until the next observation). A notional illustration of the SMPC logic is shown in Fig. 9. In the left plot, the Mahalanobis distance between the desired and propagated states is less than ϵ_{replan}, so the prior maneuver plan is maintained. In the right plot, the Mahalanobis distance is larger than ϵ_{replan}, so the maneuver plan is recomputed.

The SMPC uses two modes (which determine the update frequency and maneuver planning algorithm) depending on how much time remains until the start of the next observation. These modes are hereafter called long-term and short-term control.

Long-term control is used when the time until the next observation is at least 10 minutes (over which time the effects of natural relative motion dynamics can be complex). The objective of the long-term control mode is to "front load" the corrective maneuvers, thereby minimizing the size and corresponding errors in maneuvers performed shortly before the next observation. In this mode, the maneuver plan is updated using a recently developed fuel-optimal impulsive control algorithm for linear time-variant systems [14]. This algorithm is used to produce a set of 3–6 impulses that reach the desired relative orbit with the last maneuver performed at least 10 minutes before the start of the observation. Additionally, the total Δv cost of these maneuvers is guaranteed to be within a user-specified threshold of the minimum-possible Δv cost. The maneuver plan is checked every 10 minutes to minimize computation effort. While this algorithm introduces nondeterministic behaviors, these effects are limited by the fact that the controller is used to track a slowly varying passively safe relative orbit.

Short-term control is used when the time until the next observation is less than 10 minutes (over which time the effects of natural relative motion are simple). The objective of the short-term control is to maximize control accuracy during the science observation. This is accomplished by checking the maneuver plan every 30 s (limited by the settling time of the attitude control system) and using a Lambert solver to compute a set of two maneuvers. The first maneuver is performed as soon as possible (nominally 30 s after computation of the maneuver plan) and the second maneuver is performed as late as possible (30 s before the next observation and at least 30 s after the first maneuver). The Lambert solver is preferred over the optimal impulsive control algorithm because it allows rapid updates at minimal computation cost.

The maximum size of a single maneuver will be limited to 2 mm/s to ensure passive safety and ensure that the maneuver plan can be performed regardless of the temperature of the propulsion system.

V. Mission Concept of Operations

The VISORS mission will require significant time to downlink science data to the ground in between sets of science observations. With this in mind, the VISORS concept of operations was developed to minimize operations load on key spacecraft subsystems (avionics, power, propulsion, etc.) when not actively performing science observations. For GNC purposes, mission operations can be divided into five modes as illustrated in Fig. 10. Nominal operations are shown in black and contingencies are indicated in red.

These operations modes make extensive use of relative eccentricity/inclination vector separation for passive safety [10] and closed-form station-keeping and formation reconfiguration maneuver sequences with flight heritage on PRISMA [11] and TanDEM-X [12] when possible. The main exception is science mode, which requires new navigation and control techniques to meet the challenging science observation requirements. A high-level overview of GNC functions in nominal operations is provided in the next section, followed by a description of the safety plan.

A. Nominal Operations

The GNC modes used in nominal operations include manual mode, standby mode, transfer mode, and science mode. A summary of key operational characteristics (e.g., relative orbit geometry, frequency of

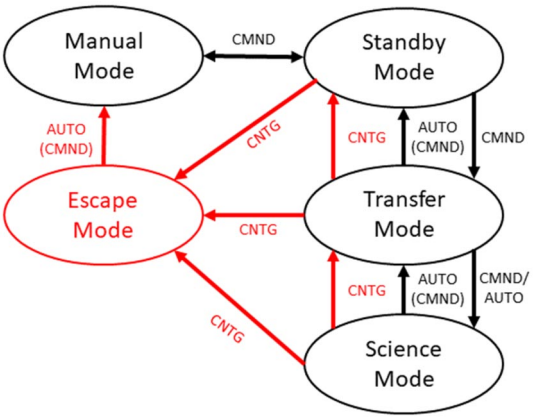

Fig. 10 GNC operations modes including nominal (black) and contingencies (red). Transitions between these modes occur by command from the ground (CMND), autonomously (AUTO), and in contingencies (CNTG).

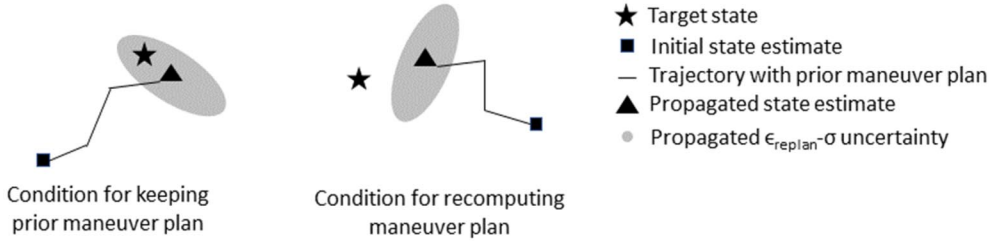

Fig. 9 Notional illustration of conditions for maintaining prior maneuver plan (left) and recomputing the maneuver plan (right) using the VISORS SMPC.

maneuvers, expected Δv costs, etc.) in each of these modes is provided in the following.

1. Manual Mode

In manual mode both of the VISORS spacecraft are controlled independently from the ground. Manual mode is used 1) at the start of the mission during initial checkout and formation acquisition, 2) after a collision avoidance maneuver until nominal capabilities are restored, and 3) at the end of the mission for decommissioning. This mode is exited to standby mode by command from the ground once communication over the ISL is established. It is expected that the formation will remain in manual mode for periods of several days to enable efficient formation acquisition from a large initial separation.

The relative orbit in manual mode is expected to have a large initial along-track separation (>10 km). The ground computes a reconfiguration maneuver sequence using conventional four-impulse solutions (three in-plane and one out-of-plane) with flight heritage on PRISMA [11] and other missions to acquire the standby mode relative orbit. It is expected that the Δv cost for initial formation acquisition will be approximately 1 m/s and the Δv cost of other manual mode instances will be less. This maneuver sequence establishes a safe separation in the plane perpendicular to the flight direction using relative eccentricity/inclination vector separation [10] before reducing the along-track separation.

2. Standby Mode

The majority of the mission is spent in standby mode, which is used for downlinking science data and waiting for science opportunities with relaxed navigation and control requirements. Standby mode is entered by command from the ground from manual mode or autonomously from transfer mode once the maneuver sequence is complete. The formation is expected to remain in standby mode for a few days to a few weeks.

The relative orbit in standby mode provides a 200 m separation in the plane perpendicular to the flight direction and an along-track separation of <5 km with a minimal drift rate to ensure that the spacecraft separation does not exceed the ISL communication range. This design provides at least several days of passive safety, allowing the formation to operate with reduced navigation accuracy (using only GNSS pseudorange measurements from both spacecraft) and minimize the frequency of station-keeping maneuvers. The mean relative eccentricity and inclination vectors are oriented along the y axis to minimize the effects of the Earth oblateness perturbation. The relative motion in the RTN frame in standby mode is illustrated in Fig. 11 (left).

Station-keeping maneuvers will be required once every several days to preserve the minimum separation in the plane perpendicular to the flight direction. This is accomplished using the aforementioned closed-form four-impulse maneuver sequence [19]. These maneuvers can be planned on the ground as a backup in case of anomalies. The in-plane maneuvers counteract the rotation of the relative eccentricity vector due to J_2 and the along-track drift due to differential atmospheric drag. The out-of-plane maneuver instead counteracts the effects of small perturbations such as third-body gravity from the sun and moon and solar radiation pressure. A notional illustration of the trajectory followed in standby mode in ROE space is shown in Fig. 11 (right). The blue dashed lines indicate the passive drift that occurs over several days. The solid red arrows indicate the instantaneous changes due to maneuvers, and the red dashed lines indicate the passive drifts between these maneuvers. As indicated in the plot of the trajectory in relative eccentricity vector space, the triplet of in-plane maneuvers are all executed during passes over the equator ($u = 0°$ or 180°). The location of the out-of-plane maneuver depends on the accumulated drift due to small perturbations.

Because the spacecraft have similar attitudes in nominal operations, the Δv cost is dominated by the rotation of the relative eccentricity vector and can be approximated by

$$\frac{\Delta v}{\Delta t} = \frac{na\delta e \sin(\dot{\omega}\Delta t/2)}{\Delta t} \leq \dot{\omega} na\delta e/2 \tag{13}$$

In a sun-synchronous orbit, the drift rate of the argument of perigee is 6.98×10^{-7} rad/s. From Eq. (13), the standby mode formation-keeping Δv cost for a nominal relative eccentricity vector of 200 m is 46 mm/s per week. If one spacecraft is tumbling due to an anomaly for an extended period of time (resulting in a large differential ballistic coefficient) and the formation is at low altitude (~500 km), the Δv cost of counteracting differential drag effects can be as large as 11 cm/s per week. This value is used to add a degree of conservatism to the mission Δv budget.

3. Transfer Mode

The main function of transfer mode is to reconfigure the formation between the required relative orbits for standby and science modes over a period of several orbits. This mode is entered from standby mode upon command from the ground or from science mode upon completion of the commanded number of observation attempts. Transfer mode is exited autonomously upon completion of a reconfiguration to standby mode. Transfer mode is exited to science mode upon command from the ground after verification that all systems are performing as expected. Once confidence in the GNC system has been established, the transition from transfer to science mode can be made autonomous.

Because the relative eccentricity and inclination vectors lie on the y axis in standby mode and near the x axis in science mode (see Fig. 6), the formation reconfiguration maneuvers must simultaneously scale and rotate the relative eccentricity and inclination vectors while maintaining passive safety at all times. These requirements can be met using the deterministic maneuver sequence described in the following. A triplet of maneuvers (two in-plane and one out-of-plane) is executed every orbit. The in-plane maneuvers are executed a half-orbit apart with one maneuver in the flight direction and the other in the antiflight direction to rotate the relative eccentricity vector while keeping the relative semimajor axis small. The out-of-plane maneuver serves to keep the relative inclination vector nearly parallel to the relative eccentricity vector throughout this transition. The magnitudes and locations of these maneuvers are selected to drive the relative eccentricity and inclination vectors in a straight line from their nominal configurations in standby mode to the required values for science mode (or vice versa), minimizing Δv expenditure [19]. The number and magnitudes of these maneuvers are selected to satisfy three constraints: 1) the relative semimajor axis never exceeds a user-specified fraction of the relative eccentricity vector magnitude, 2) the angle between the relative eccentricity and inclination vector

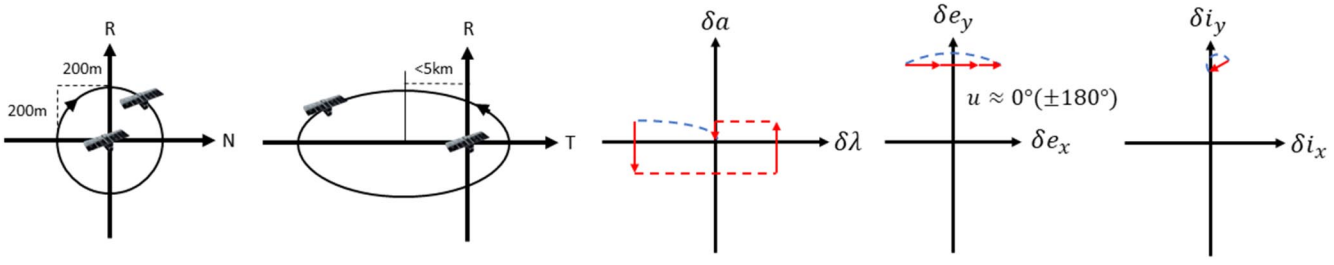

Fig. 11 Nominal standby mode relative orbit in the RTN frame (left) and station-keeping limit cycle in ROE space (right) including days of passive drift (blue), station-keeping maneuvers (red arrows), and along-track drift between station-keeping maneuvers (red dashed line).

never exceeds a user-specified maximum value, and 3) the expected maneuver execution error (which scales with maneuver magnitude) does not exceed a user-specified fraction of the nominal separation. These constraints ensure that the passive safety of the formation is maintained after every maneuver.

Figure 12 (left) shows an example transfer mode trajectory in the RN plane. It is evident from this figure that passive safety is maintained after each maneuver. A transfer mode trajectory in ROE space produced by this sequence of maneuvers is shown in Fig. 12 (right). In this example, the locations of the along-track and cross-track maneuvers are separated by 3°, and the maneuver magnitudes decrease over time to minimize the impact of maneuver execution error on passive safety. Since the magnitudes of the relative eccentricity and inclination vectors are much larger in standby mode than in science mode, it is expected that all maneuvers will occur near the poles.

The Δv cost of the formation reconfiguration is invariant of the number of maneuvers and depends primarily on the nominal separation in standby mode. The Δv cost of a single reconfiguration can be approximated as

$$\Delta v = n(0.5\|\Delta a\delta \boldsymbol{e}\| + \|\Delta a\delta \boldsymbol{i}\|) \tag{14}$$

where $\Delta a\delta \boldsymbol{e}$ and $\Delta a\delta \boldsymbol{i}$ denote the changes in the relative eccentricity and inclination vectors. If the relative eccentricity and inclination vectors have nominal magnitudes of 200 m in standby mode, the Δv cost of a formation reconfiguration from standby mode to science mode (or vice versa) is approximately 0.3 m/s.

4. *Science Mode*

Science mode is used to collect images of a target active region of the sun once per orbit. This mode is entered from transfer mode upon command from the ground (or autonomously once confidence in the GNC system is established). Science mode is exited autonomously to transfer mode once the commanded number of observation attempts have been performed. The number of consecutive observations to be performed will not exceed 15 (limited by data storage), so the formation will not remain in science mode for longer than 1 day.

When in science mode, the relative motion is autonomously controlled by the SMPC (see Sec. IV) to track a trajectory that passively satisfies the observation requirements once per orbit. The nominal relative orbit in science mode is illustrated in Fig. 13. The desired relative orbit is tracked with millimeter-level accuracy during the observation arc and an accuracy of approximately 2 m throughout the rest of the orbit. However, it should be noted that the exact relative orbit depends on β.

The Δv cost of station-keeping maneuvers during science mode is dominated by navigation, control, and modeling errors. From preliminary simulations (see Sec. VI), the maximum expected Δv per observation from conducted simulations is 26 mm/s with an average Δv cost of 12 mm/s per observation. Station-keeping requires 5–27 maneuvers per orbit, with an average maneuver size of 0.5 mm/s.

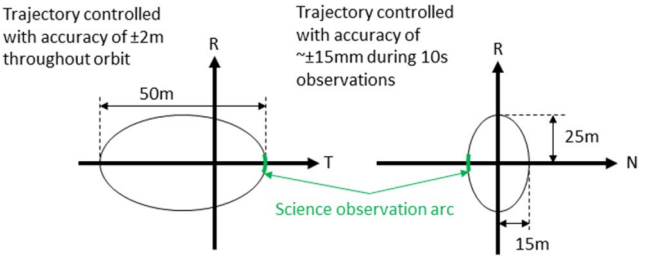

Fig. 13 Nominal science mode relative orbit in the RTN frame including observation arc (green).

5. *Δv Budget*

The Δv budget for the nominal VISORS mission plan is shown in Fig. 14. This mission plan includes 100 observation attempts divided into 10 sets. The Δv budget uses worst-case (3-σ) values for station-keeping Δv costs in science mode and standby mode. Even with this conservative assumption, 19% of the 16 m/s total Δv capacity remains unallocated. This margin suggests that VISORS can achieve mission success even if the propulsion system on one spacecraft fails during the mission.

B. Safety Plan

The VISORS safety plan includes two layers: 1) autonomous reversion to standby mode, and 2) autonomous collision avoidance using escape mode.

If the formation experiences an anomaly that prevents observation attempts (e.g., bus safe mode, outages in the ISL, GNSS receivers, or star trackers) while in transfer or science modes, the formation autonomously reverts to standby mode (see vertical red lines in Fig. 10). This ensures at least several days of passive safety while the issue is resolved by the ground. The ground can also control the spacecraft individually if the ISL is inoperative.

In the event of a more severe anomaly, the formation enters escape mode, causing the deputy spacecraft to plan and execute a single collision avoidance maneuver if possible. Escape mode is entered if the navigation algorithms indicate that the separation between the spacecraft will decrease below a user-specified threshold within two orbits. The maneuver is planned for execution at least one orbit before the separation will decrease below acceptable levels and aims to simultaneously 1) increase the radial and cross-track separations and 2) introduce an along-track drift to ensure long-term safety. An example trajectory before and after a collision avoidance maneuver in the RTN frame is illustrated in Fig. 15.

VI. Validation

To demonstrate that the VISORS mission can meet the relative motion control requirements with the required total likelihood of 20%, a set of Monte Carlo simulations were conducted including all significant error sources and constraints affecting the mission. These simulations provide quantitative estimates of the likelihood

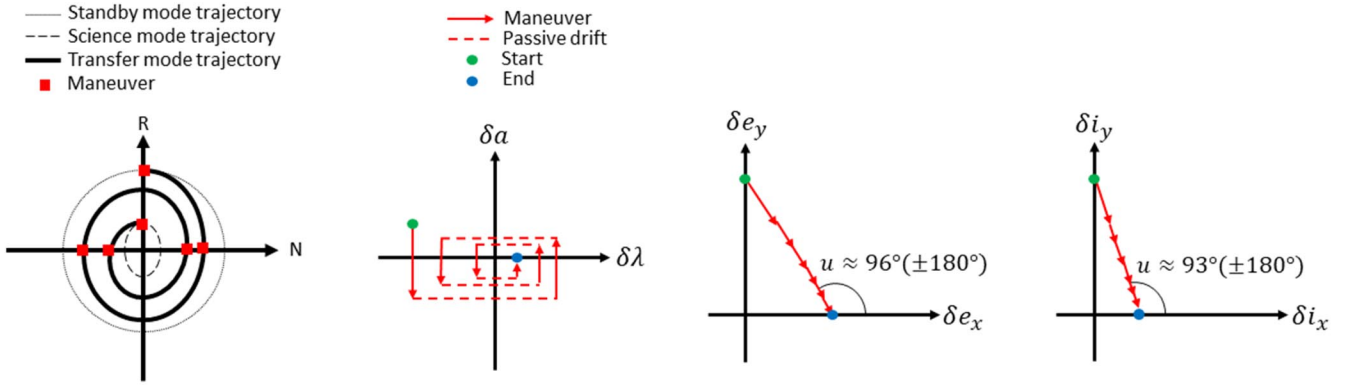

Fig. 12 Example transfer mode trajectory in the RN plane (left) and ROE space (right) with passive safety maintained at all times.

Maneuver type	ΔV (m/s)	Number of events	Total ΔV (m/s)	Contingency (%)	Max expected ΔV (m/s)
Formation acquisition	1.00	1	1.00	50	1.50
Standby mode station-keeping (1 week)	0.11	13	1.43	10	1.57
Transfer (standby to science)	0.30	10	3.00	10	3.30
Transfer (science to standby)	0.30	10	3.00	10	3.30
Science observation	0.026	100	2.60	10	2.86
Collision avoidance	0.15	1	0.15	10	0.17
Standby mode reacquisition	0.30	1	0.30	10	0.33
Total	-	-	**11.18**	**14.18**	**13.03**
				Capacity (m/s)	**16.00**
				Unallocated (m/s)	**2.97**
				Unallocated (%)	**18.56**

Fig. 14 Δv budget for nominal VISORS mission plan with 100 observation attempts.

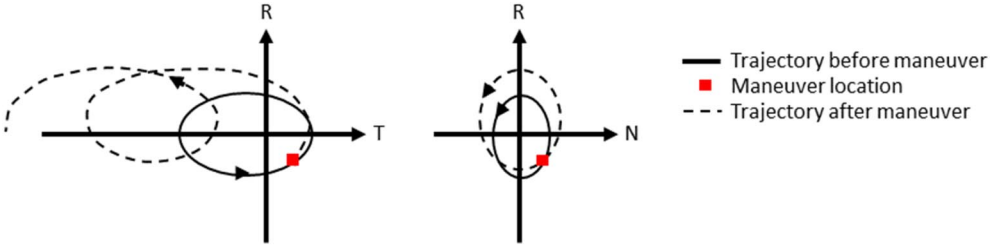

Fig. 15 Example relative motion before (solid line) and after (dashed line) a collision avoidance maneuver in the RTN frame.

of meeting each of the key GNC requirements (lateral relative position of the sieve with respect to the detector, lateral relative velocity of the sieve with respect to the detector, and the separation between the sieve and detector), as well as their sensitivity to key errors and design parameters. The only significant distinction between the mechanization of the SMPC control law used in these simulations and that described in Sec. IV is that bounds on the magnitudes of each maneuver are not enforced. However, the results of these simulations indicate a 1-σ maneuver magnitude of 0.5 mm/s, demonstrating that such a bound would have negligible impact on the computed maneuver plans.

A. Simulation Description

The initialization procedure, dynamics models, error sources, and operational constraints used in these simulations are described in the following.

1. *Initialization*

The absolute orbit for the DSC (which is assumed to be the passive chief in all simulations) is initialized by random selection from the distribution described in Table 5 to provide a representative sampling of observation scenarios. The selected altitude maximizes the effects of differential atmospheric drag, providing a degree of conservatism in the simulation results.

The relative orbit is initialized using a three-step procedure that is designed to be representative of repeated observations in science mode. First, the orbit of the DSC is propagated to the start of the science observation. Second, the desired ROEs for the OSC are computed from the DSC orbit and the pointing vector to the sun. Finally, the initial ROEs for the OSC are computed by adding a random error of 2 m (1-σ) to these desired ROEs. This is representative of the expected initial errors for repeated observation attempts as the changes in the desired ROEs over one orbit are expected to be small.

Table 5 Absolute orbit parameters

Epoch	Random epoch in 2024 (with predicted solar flux data to cause changes in atmospheric density profile)
Altitude	500 km
Inclination	98° (sun-synchronous)
LTAN	10AM (to provide passive safety)
Eccentricity	0.001
Argument of latitude	Selected based on orbit epoch to ensure that formation can be properly aligned with the sun (in the local TN plane) after one orbit

2. *Dynamics Models*

To ensure realistic simulations, it is necessary to distinguish between the ground truth dynamics model (which governs the spacecraft behavior in simulation) and the onboard dynamics model (which determines the predicted spacecraft behavior in the GNC algorithms). The key models and parameters used in these dynamics models are provided in Table 6. The main distinction between these models is that the onboard model uses a reduced geopotential model and makes a conservative assumption of overestimating atmospheric density by 1000%. For these simulations, it is assumed that the spacecraft maintain a constant inertial attitude, resulting in a differential ballistic coefficient that oscillates between 0.008 m^2/s and 0.03 m^2/s. The effects of eclipses on the solar radiation pressure perturbation are neglected because eclipses are only a few minutes in duration for an LTAN of 10AM. The numerical integrator uses Gauss's variational equations to enable use of 30 s time steps without compromising propagation accuracy [20].

3. *Error Sources and Operational Constraints*

The simulations include navigation errors, actuation errors, and operational constraints that are consistent with the selected hardware and software. The error values and operational constraints are provided in Table 7. The navigation and maneuver execution errors at

Table 6 Ground truth and onboard dynamics model parameters

Parameter	Ground truth	Onboard
Geopotential	60 × 60 GGMOS1 [1]	10 × 10 GGMOS1 [1]
Atmospheric density	NRLMSISE-00 [15]	NRLMSISE-00 [15] (with constant 1000% error)
Third-body gravity	Analytical lunisolar ephemerides	Analytical lunisolar ephemerides
Solar radiation pressure	Cannonball model, no eclipses	Cannonball model, no eclipses
Integrator	RK4 with 30 s time step	RK4 with 30 s time step

Table 7 Errors of 1-σ from DiGiTaL [5] and propulsion [6] and other system parameters

Navigation errors (1-σ, per axis) [5]			
Absolute position	1 m	Relative position	1 cm
Absolute velocity	1 cm/s	Relative velocity	25 μm/s
Actuation errors [6] and parameters			
Minimum impulse bit	1e-3 N · s	Minimum impulse increment	6e-5 N · s
Maneuver execution error (1-σ)	5%	Attitude settling time	30 s
Maneuver direction error (1-σ)	1 arcmin	Spacecraft mass	12 kg

each time step in the simulation are computed by sampling from a zero-mean Gaussian distribution with the corresponding uncertainties. The effects of nonzero-mean error distributions can be inferred from the sensitivity study (which includes double and triple the nominal error values). The navigation errors are assumed to be identical for each axis at this stage of the design process for simplicity. More precise error estimates for the orbit and attitude estimation capabilities will be generated later in the design process using test results from hardware-in-the-loop testbeds.

To avoid any misinterpretation, the minimum impulse bit is the smallest maneuver that can be executed by the propulsion system and the minimum impulse increment is the minimum amount a maneuver can be increased beyond the minimum impulse bit (due to constraints on valve timing in the propulsion system). The attitude settling time is both the minimum time between consecutive maneuvers and the minimum time between the final maneuver and an observation.

B. Simulation Error Metrics

The control performance is evaluated by three error metrics: 1) the maximum longitudinal relative position error during the observation, 2) the maximum lateral relative position error during the observation, and 3) the maximum lateral relative velocity error during the observation. These error metrics are computed in two steps. First, the relative motion during the observation is simulated by numerically propagating the absolute and relative orbits of the VISORS spacecraft for 10 s in 1 s steps using the ground truth dynamics model. Second, the error metrics are computed by taking the maximum of each error over the 11 sample times. For a successful observation, these error metrics should be less than the values provided in Table 8.

Table 8 Maximum error metrics for successful observation

Parameter	Value
Longitudinal relative position control	15 mm
Lateral relative position control	18 mm
Lateral relative velocity control	0.2 mm/s

C. Results

Monte Carlo experiments were conducted to characterize the likelihood of meeting each of the control requirements and the sensitivity of these likelihoods to key error sources and mission parameters. The selected key parameters include absolute navigation error, relative navigation error, maneuver execution error, and attitude settling time. For each set of mission parameters and error values, a set of 100 simulations was conducted. These simulations are used to produce a cumulative distribution function (CDF) for each of the error metrics. The CDFs for the error metrics in nominal simulations are shown in Fig. 16.

It can be seen from these plots that the likelihood of meeting the range requirement is 87%, the likelihood of meeting the lateral relative position requirement is 77%, and the lateral relative velocity requirement is satisfied in every simulation. Under the assumption that these errors are uncorrelated, the likelihood of meeting all three requirements simultaneously is 67%, which agrees with the simulation results (all three requirements were met in 67 of the 100 simulations). This provides significant margin over the required 20% success rate.

The CDFs of the total required Δv and the number of maneuvers performed in each simulation are shown in Fig. 17. On average, each observation requires approximately 17 maneuvers at a total Δv cost of 12 mm/s. The maximum Δv cost for a single observation was 26 mm/s.

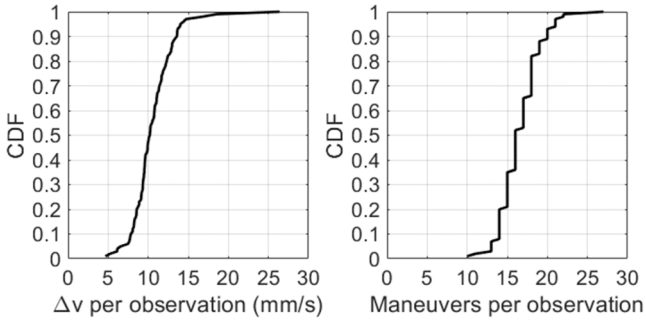

Fig. 17 CDFs for longitudinal relative position (left), lateral relative position (middle), and lateral relative velocity (right) control error metrics with nominal errors and operational constraints.

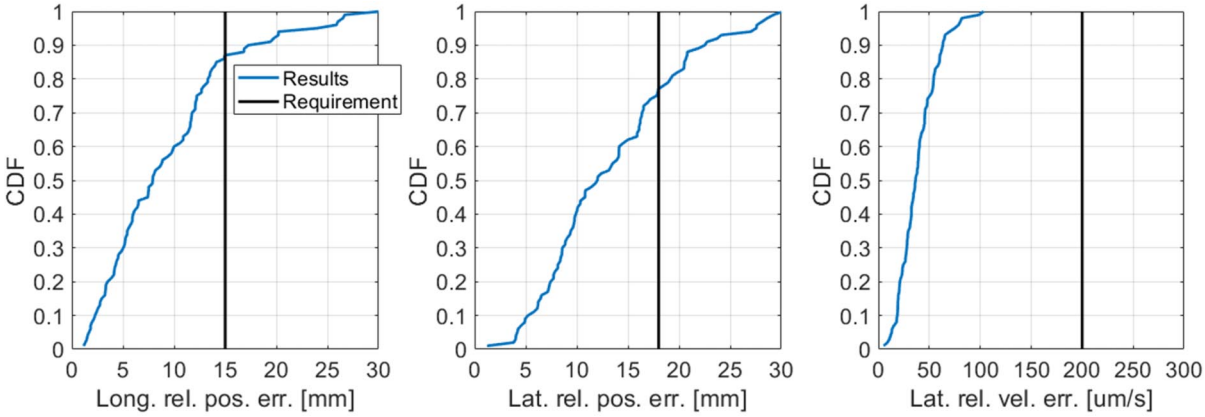

Fig. 16 Nominal control error metric CDFs for longitudinal relative position (left), lateral relative position (middle), and lateral relative velocity (right).

1. Absolute Navigation Error Sensitivity

The sensitivity of the performance to absolute navigation errors was assessed by repeating simulations with the absolute navigation errors doubled and tripled with respect to the nominal values. Figure 18 shows the superimposed error metric CDFs for the three simulation sets. As the CDFs are effectively identical, it is clear that performance is insensitive to absolute navigation errors.

2. Relative Navigation Error Sensitivity

The sensitivity of the performance to relative navigation errors was assessed by repeating simulations with the relative navigation errors doubled and tripled. Figure 19 shows the superimposed CDFs for the three simulation sets. It is evident that each of the CDFs is roughly proportional to the applied errors, suggesting that relative navigation errors are a key driver of the control performance. As such, it is important to verify that the modeled relative navigation accuracy is achievable as the mission design matures. It should be noted that all three requirements were satisfied in 16% of simulations with doubled relative navigation errors, which suggests that an increase of approximately 70% in the 1-σ relative navigation error is acceptable while meeting the 20% observation success likelihood requirement.

3. Maneuver Execution Sensitivity

The sensitivity of the performance to maneuver execution errors was assessed by repeating simulations with the maneuver execution errors (both direction and magnitude error) doubled and tripled. The superimposed CDFs from the three simulation sets are shown in Fig. 20. It is evident that the increased maneuver execution error has negligible effect on the control accuracy. Specifically, tripling the maneuver execution errors only reduces the success rate from 67 to

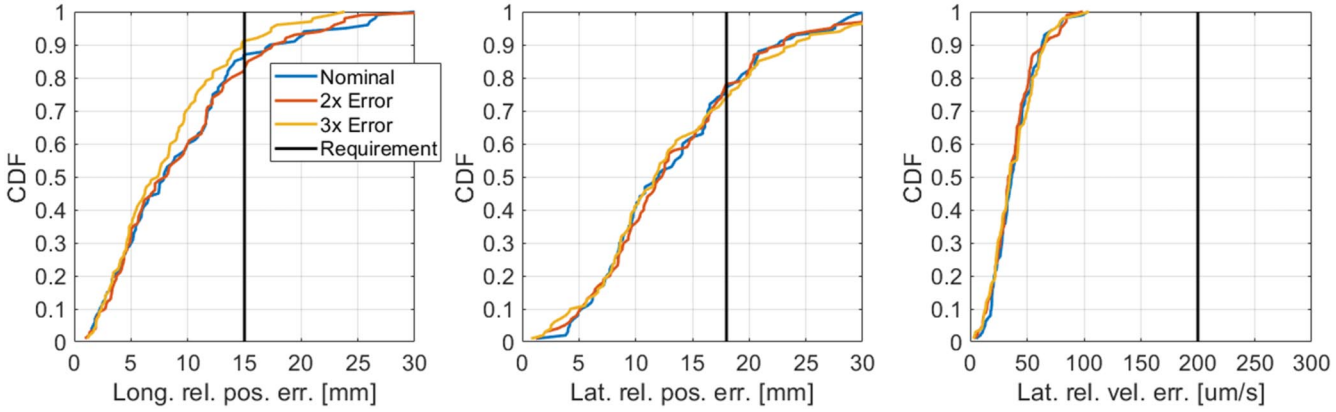

Fig. 18 Comparison of error metric CDFs for nominal, double, and triple absolute navigation errors.

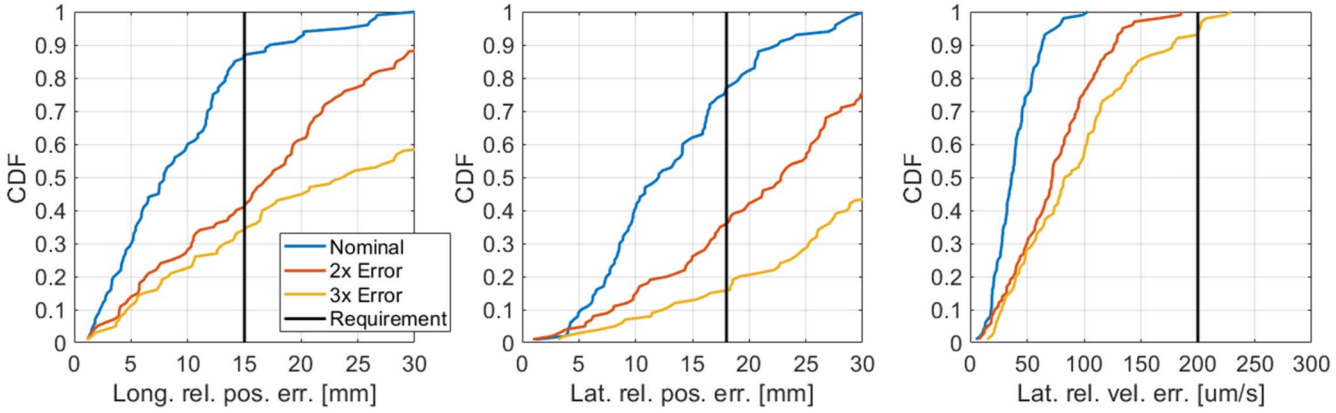

Fig. 19 Comparison of error metric CDFs for nominal, double, and triple relative navigation errors.

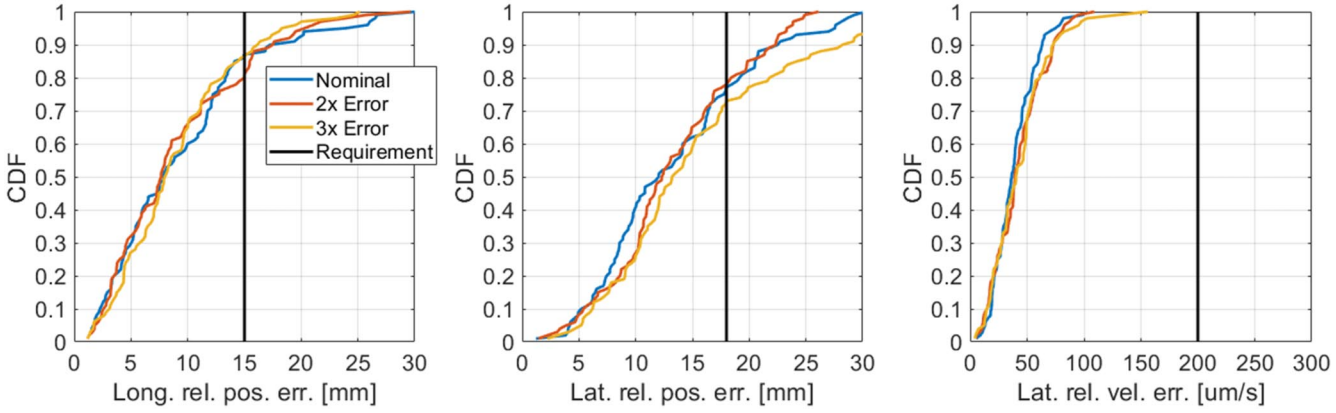

Fig. 20 Comparison of error metric CDFs for simulations with nominal, double, and triple maneuver execution errors.

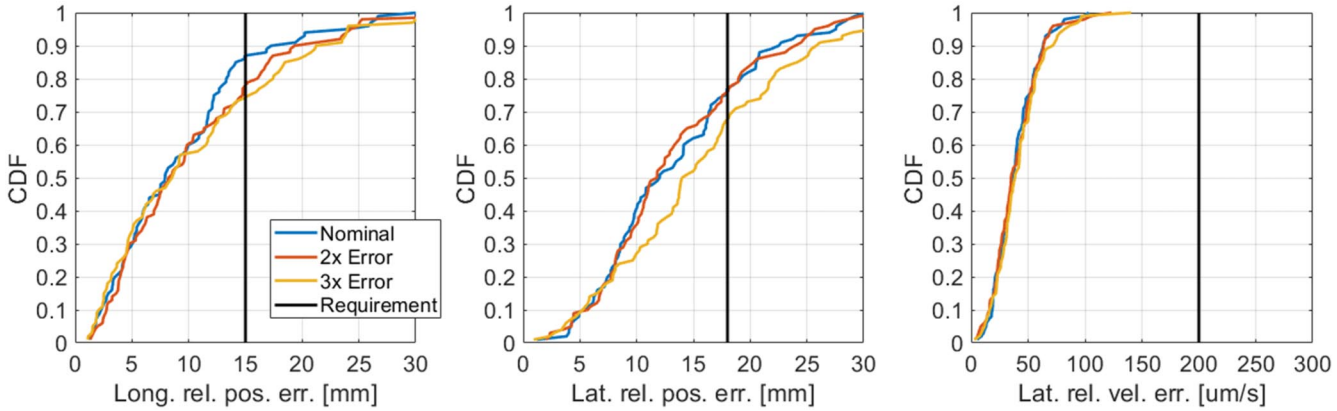

Fig. 21 Comparison of error metric CDFs for simulations with nominal, double, and triple the maneuver update sample time and minimum time from the final maneuver to the observation.

64%. This is because the effect of maneuver execution errors at these levels is still small compared to the effects of relative navigation errors.

4. Settling Time Sensitivity

The sensitivity of the performance to the settling time of the attitude control system (which drives the minimum time between maneuvers and the minimum time between the final maneuver and observation) was assessed by repeating simulations with this value doubled and tripled. The CDFs of the three simulation sets are shown in Fig. 21. It is evident that increasing these times causes a small increase in the relative position errors. Specifically, tripling the settling time reduces the success rate from 67 to 48%. This behavior is expected as an instantaneous error in the relative velocity causes an accumulation of relative position error over time. However, it is evident that an increase in the settling time (e.g., due to degraded reaction wheel performance) or reducing the frequency of maneuver plan updates (e.g., due to processing power limits) does not pose a significant risk to mission success.

VII. Conclusions

This paper addressed the design of the absolute and relative orbits; guidance, navigation, and control system; and concept of operations for the VISORS mission. VISORS will use a distributed telescope consisting of 6U CubeSats deployed in low Earth orbit to collect high-resolution images of the sun in the extreme ultraviolet spectrum. To meet the challenging requirements posed by the telescope instrument, the CubeSats will autonomously control their relative motion with millimeter-level accuracy. However, the designs proposed in this paper can be used for other distributed telescopes or CubeSat missions that require accurate and autonomous formation control with minimal modification.

First, it was demonstrated that a subset of passively safe relative orbits based on relative eccentricity/inclination vector separation provide periods of natural alignment with inertial targets. These relative orbits are obtained by simply ensuring that observations are centered about times when the pointing vector to the target lies in the local tangential/normal plane and that the tangential and normal components of the pointing vector are both nonzero. Additionally, it was shown that there are two windows at least 1 minute in duration in any low Earth orbit during which the lateral relative acceleration at 40 m separation is no larger than 5 μm/s, ensuring that the natural relative motion accounts for no more than 25% of the lateral relative velocity control error budget for VISORS science observations. The selected orbit for VISORS is a sun-synchronous low Earth orbit with an altitude of at least 500 km to enable persistent use of these relative orbits. This orbit is easily accessible for secondary payloads and provides slow and predictable variations of the beta angle over the year. The local time of the ascending node can take on any value in the 1–4AM/PM or 8–11AM/PM ranges while ensuring at least two orbits of passive safety.

Each VISORS spacecraft is equipped a guidance, navigation, and control system that is compatible with the size, weight, power, and computation limits of 6U CubeSats. The selected hardware includes a dual-frequency GNSS receiver and antenna, a near-omnidirectional intersatellite link, and an omnidirectional cold-gas propulsion system. These components ensure that relative navigation and control capabilities are retained in a wide range of relative orbits and attitudes. The software includes assignable chief and deputy roles to disambiguate control authority, ensuring safe and predictable operations in the event of communication outages. Overall, the guidance, navigation, and control system provides autonomous navigation and control with millimeter-level accuracy, enabling VISORS science observations.

The VISORS concept of operations was developed to minimize operations load on key subsystems when not actively performing observations. After initial formation acquisition, nominal operations are divided between standby, transfer, and science modes. Standby and transfer modes are based on heritage approaches and algorithms, while science mode features novel navigation and maneuver planning algorithms to enable millimeter-level control accuracy. Specifically, standby mode provides days of passive safety with sparse station-keeping maneuvers, allowing the formation to downlink science data and wait for observation opportunities. Transfer mode provides passively safe formation reconfigurations between standby and science modes using closed-form maneuver plans executed over several orbits. In science mode, navigation estimates are computed using differential carrier-phase GNSS techniques that provide 1-σ relative position and velocity errors of 1 cm and 0.025 mm/s, respectively. These solutions are used in a stochastic model predictive controller that ensures that the formation is aligned with the target once per orbit.

The performance of the guidance, navigation, and control system was validated through Monte Carlo simulations including representative error sources and operational constraints. Each simulation is successful if the maximum errors in the longitudinal relative position, lateral relative position, and lateral relative velocity over the 10 s observation are within the prescribed limits of 15 mm, 18 mm, and 0.2 mm/s respectively. It was found that all three requirements were met in 67% of observation attempts with nominal errors, providing ample margin over the required 20% success likelihood. Additionally, the Δv cost per observation was found to be no larger than 26 mm/s. The simulations were repeated to characterize the sensitivity of the performance to navigation and control errors as well as the settling time of the attitude control system. These simulations demonstrated that the performance primarily depends on the relative navigation accuracy, which will need to be validated through more thorough testing as the VISORS mission design matures.

Overall, these results provide a preliminary demonstration of the technical feasibility of meeting the challenging relative motion control requirements the VISORS mission. Additionally, the new orbit and guidance, navigation, and control system designs can be applied to other distributed telescopes and CubeSat formation flying missions

with minimal modification, enabling compelling science at a small fraction of the cost of flagship-class missions.

Acknowledgments

The authors would like to acknowledge NSF Award #1936663 and the VISORS team for their insight and contributions to the mission design, requirements definition, illustrations, and system modeling. The authors would particularly like to thank Farzad Kamabaladi, Doug Rabin, Adrain Daw, Hyeongjun Park, and Alina Alexeenko.

References

[1] Tapley, B. D., Bettadpur, S., Watkins, M., and Reigber, C., "The Gravity Recovery and Climate Experiment: Mission Overview and Early Results," *Geophysical Research Letters*, Vol. 31, No. 9, 2004, pp. 1–4, https://agupubs.onlinelibrary.wiley.com/doi/10.1029/2004GL019920. https://doi.org/10.1029/2004GL019920

[2] Krieger, G., Moreira, A., Fiedler, H., Hajnsek, I., Werner, M., Younis, M., and Zink, M., "TanDEM-X: A Satellite Formation for High-Resolution SAR Interferometry," *IEEE Transactions on Geoscience and Remote Sensing*, Vol. 45, No. 11, 2007, pp. 3317–3341. https://doi.org/10.1109/TGRS.2007.900693

[3] Burch, J., Moore, T., Torbert, R., and Giles, B., "Magnetospheric Multiscale Overview and Science Objectives," *Space Science Reviews*, Vol. 199, Nos. 1–4, 2016, pp. 5–21. https://doi.org/10.1007/s11214-015-0164-9

[4] Palo, S., Stafford, G., and Hoskins, A., "An Agile Multi-Use Nano Star Camera for Constellation Applications," *Proceedings of the AIAA/USU Conference on Small Satellites*, Mission Lessons, SSC13-XIII-5, 2013, https://digitalcommons.usu.edu/smallsat/2013/all2013/63/.

[5] Giralo, V., and D'Amico, S., "Distributed Multi-GNSS Timing and Localization for Nanosatellites," *Navigation*, Vol. 66, No. 4, 2019, pp. 729–746. https://doi.org/10.1002/navi.337

[6] Lightsey, E. G., Stevenson, T., and Sorgenfrei, M., "Development and Testing of a 3-D-Printed Cold Gas Thruster for an Interplanetary CubeSat," *Proceedings of the IEEE*, Vol. 106, No. 3, 2018, pp. 379–390. https://doi.org/10.1109/JPROC.2018.2799898

[7] Kamabaladi, F., Alexeenko, A., Chamberlin, P., D'Amico, S., Daw, A., Denis, K., Ekici, E., Gupta, S., Hwang, J., Klimchuk, J., et al., "Collaborative Research: CubeSat Ideas Lab: VIrtual Super-Resolution Optics with Reconfigurable Swarms (VISORS)," 2019, https://www.nsf.gov/awardsearch/showAward?AWD_ID=1936663.

[8] Llorente, J. S., Agenjo, A., Carrascosa, C., de Negueruela, C., Mestreau-Garreau, A., Cropp, A., and Santovincenzo, A., "PROBA-3: Precise Formation Flying Demonstration Mission," *Acta Astronautica*, Vol. 82, No. 1, 2013, pp. 38–46. https://doi.org/10.1016/j.actaastro.2012.05.029

[9] Koenig, A. W., Macintosh, B., and D'Amico, S., "Formation Design of Distributed Telescopes in Earth Orbit for Astrophysics Applications," *Journal of Spacecraft and Rockets*, Vol. 56, No. 5, 2019, pp. 1462–1477. https://doi.org/10.2514/1.A34420

[10] D'Amico, S., and Montenbruck, O., "Proximity Operations of Formation-Flying Spacecraft Using an Eccentricity/Inclination Vector Separation," *Journal of Guidance, Control, and Dynamics*, Vol. 29, No. 3, 2006, pp. 554–563. https://doi.org/10.2514/1.15114

[11] D'Amico, S., "Autonomous Formation Flying in Low Earth Orbit," Ph.D. Thesis, Delft Univ., Delft, The Netherlands, 2010.

[12] Montenbruck, O., Kahle, R., D'Amico, S., and Ardaens, J.-S., "Navigation and Control of the TanDEM-X Formation," *Journal of the Astronautical Sciences*, Vol. 56, No. 3, 2008, pp. 341–357. https://doi.org/10.1007/BF03256557

[13] Koenig, A. W., Guffanti, T., and D'Amico, S., "New State Transition Matrices for Spacecraft Relative Motion in Perturbed Orbits," *Journal of Guidance, Control, and Dynamics*, Vol. 40, No. 7, 2017, pp. 1749–1768. https://doi.org/10.2514/1.G002409

[14] Koenig, A. W., and D'Amico, S., "Fast Algorithm for Fuel-Optimal Impulsive Control of Linear Systems with Time-Varying Cost," *IEEE Transactions on Automatic Control*, Vol. 66, No. 9, 2020, pp. 4029–4042. https://doi.org/10.1109/TAC.2020.3027804

[15] Picone, J., Hedin, A., Drob, D. P., and Aikin, A., "NRLMSISE-00 Empirical Model of the Atmosphere: Statistical Comparisons and Scientific Issues," *Journal of Geophysical Research: Space Physics*, Vol. 107, No. A12, 2002, pp. SIA 15-1–SIA 15-16. https://doi.org/10.1029/2002JA009430

[16] Gundamraj, A. R., Thatavarthi, R., Carter, C., Lightsey, E. G., Koenig, A., and D'Amico, S., "Preliminary Design of a Distributed Telescope CubeSat Formation for Coronal Observations," *AIAA Scitech 2021 Forum*, AIAA Paper 2020-0422, 2020. https://doi.org/10.2514/6.2021-0422

[17] Ardaens, J.-S., and Fischer, D., "TanDEM-X Autonomous Formation Flying System: Flight Results," *IFAC Proceedings Volumes*, Vol. 44, No. 1, 2011, pp. 709–714. https://doi.org/10.3182/20110828-6-IT-1002.02374

[18] Giralo, V., Chernick, M., and D'Amico, S., "Guidance, Navigation, and Control for the DWARF Formation-Flying Mission," *Astrodynamics 2020 Advances in the Astronautical Sciences, Proceedings of the AAS/AIAA Astrodynamics Specialist Conference*, Vol. 175, Univelt Inc., 2020, pp. 3893–3912; also AAS Paper 20-560, 2020.

[19] Chernick, M., and D'Amico, S., "New Closed-Form Solutions for Optimal Impulsive Control of Spacecraft Relative Motion," *Journal of Guidance, Control, and Dynamics*, Vol. 41, No. 2, 2018, pp. 301–319. https://doi.org/10.2514/1.G002848

[20] Sullivan, J. A., "Nonlinear Angles-Only Orbit Estimation for Autonomous Distributed Space Systems," Ph.D. Thesis, Stanford Univ., Stanford, CA, 2020.